
This is an electronic reprint of the original article.
This reprint may differ from the original in pagination and typographic detail.

Miranda-Valdez, Isaac Yair; Mäkinen, Tero; Hu, Xiang; Lejon, Juha; Elamir, Mohamed; Viitanen, Leevi; Jannuzzi, Luisa; Koivisto, Juha; Alava, Mikko Juhani

Bio-Based Foams to Function as Future Plastic Substitutes by Biomimicry : Inducing Hydrophobicity with Lignin

Published in:
Advanced Engineering Materials

DOI:
[10.1002/adem.202400233](https://doi.org/10.1002/adem.202400233)

Published: 01/10/2024

Document Version
Publisher's PDF, also known as Version of record

Published under the following license:
CC BY

Please cite the original version:
Miranda-Valdez, I. Y., Mäkinen, T., Hu, X., Lejon, J., Elamir, M., Viitanen, L., Jannuzzi, L., Koivisto, J., & Alava, M. J. (2024). Bio-Based Foams to Function as Future Plastic Substitutes by Biomimicry : Inducing Hydrophobicity with Lignin. *Advanced Engineering Materials*, 26(20), Article 2400233.
<https://doi.org/10.1002/adem.202400233>

This material is protected by copyright and other intellectual property rights, and duplication or sale of all or part of any of the repository collections is not permitted, except that material may be duplicated by you for your research use or educational purposes in electronic or print form. You must obtain permission for any other use. Electronic or print copies may not be offered, whether for sale or otherwise to anyone who is not an authorised user.

Bio-Based Foams to Function as Future Plastic Substitutes by Biomimicry: Inducing Hydrophobicity with Lignin

Isaac Yair Miranda-Valdez, Tero Mäkinen,* Xiang Hu, Juha Lejon, Mohamed Elamir, Leevi Viitanen, Luisa Jannuzzi, Juha Koivisto, and Mikko Juhani Alava

To replace common plastics, bio-based alternatives are needed. Cellulose foams, as plant-based materials, are the most attractive solution, being often biodegradable and inexpensive and having the potential for distributed production. Cellulose and its derivatives, as raw materials, present a fundamental challenge, as they are hydrophilic. Herein, this problem is solved by drawing inspiration from the hydrophobic barrier that lignin creates in wood and applying lignin to methylcellulose (MC) foams. The lignin (0.0–1.0 wt% being the range studied here) is applied directly to the suspension consisting of water and MC (1.8 wt%), which is then foamed and solidified to a dry 3D porous structure. By comparing different types of lignin and the resulting surface morphologies, it is shown that organosolv lignin (OL) most strongly self-assembles to the air–foam interfaces, achieving area fractions up to 27%. Using different concentrations of OL, how hydrophobicity—described by the initial water contact angle and its time evolution—increases with increasing lignin concentration is then shown. Thus, significantly increased water resistance (up to 91 times higher compared to the pure MC foam), a crucial property for developing novel bio-based materials that can compete with traditional plastics, is able to be achieved.

innovations in packaging, buildings, electronics, and medicine.^[2,3] Cellulose is a mechanically strong, chemically accessible, biodegradable, and low-density material, making it suitable for use in packaging. Thus, it is of growing interest as a building block for alternatives to plastic foams.^[4–12] The use of cellulose foams as alternatives is nevertheless limited, since these foams lack resistance to wetting or water in general. In this study, we used biomimicry to exploit the properties of lignin, one of the most abundant natural polymers, to design foams from a cellulose derivative and lignin. They achieved hydrophobic properties, allowing them to break through the barriers that have prevented them from being used as real plastic substitutes.

In principle, cellulose-based foams (or simply cellulose foams) are 3D porous structures inspired by the cellular architecture of wood, as shown in **Figure 1a**.^[12–14] Cellulose foam manufacturing typically follows a liquid templating process during

which the foam develops an open or closed cell structure.^[12,15–18]

We have previously shown that, by using a specific manufacturing process, the foams can have an elongated cell structure^[11,12,19] reminiscent of the cellular structure of wood. Although the structure of lignocellulosic cell walls in wood is complex, it is worthwhile to follow further lessons from its structure, exploiting the lignin wood contains to imitate the synergy arising from lignin embedded in wood. In wood lignin acts as a hydrophobic barrier, preventing cellulose degradation and microbial attacks.^[20] Thus far, lignin has not been exploited to hydrophobize cellulose-based materials on a practical scale,^[7] although efforts have been made with aerogels^[21–23] and films.^[24–26] This is because isolated lignin undergoes drastic structural changes compared with its native chemistry when present in wood.^[27,28] Although commercial lignin is available in large amounts as a by-product of wood pulping, it possesses a complex chemical structure that makes its valorization challenging.^[27] Accordingly, a most important and puzzling question arises of whether valorizing lignin as an additive for foams based on cellulose derivatives is possible.

Producing foams through liquid templating allows interfacial phenomena to be taken advantage of in the air–liquid boundaries. In fact, driving particles such as silica and cellulose fibers to the air–liquid interfaces is a recurrent technique to modify the

1. Introduction

The increasing concern about plastics as marine pollution has led policymakers to establish new directives limiting the use of plastic products.^[1] Such directives entail material selection and design challenges, and natural polymers would be an obvious solution for replacing plastics. Cellulose, a natural polymer present mainly in the cell walls of plants, is abundant and readily available in nature^[2] and is becoming increasingly exploited in

I. Y. Miranda-Valdez, T. Mäkinen, X. Hu, J. Lejon, M. Elamir, L. Viitanen, L. Jannuzzi, J. Koivisto, M. J. Alava
Department of Applied Physics
Aalto University
P.O. Box 15600, Aalto, FI-00076 Espoo, Finland
E-mail: tero.j.makinen@aalto.fi

 The ORCID identification number(s) for the author(s) of this article can be found under <https://doi.org/10.1002/adem.202400233>.

© 2024 The Author(s). Advanced Engineering Materials published by Wiley-VCH GmbH. This is an open access article under the terms of the Creative Commons Attribution License, which permits use, distribution and reproduction in any medium, provided the original work is properly cited.

DOI: 10.1002/adem.202400233

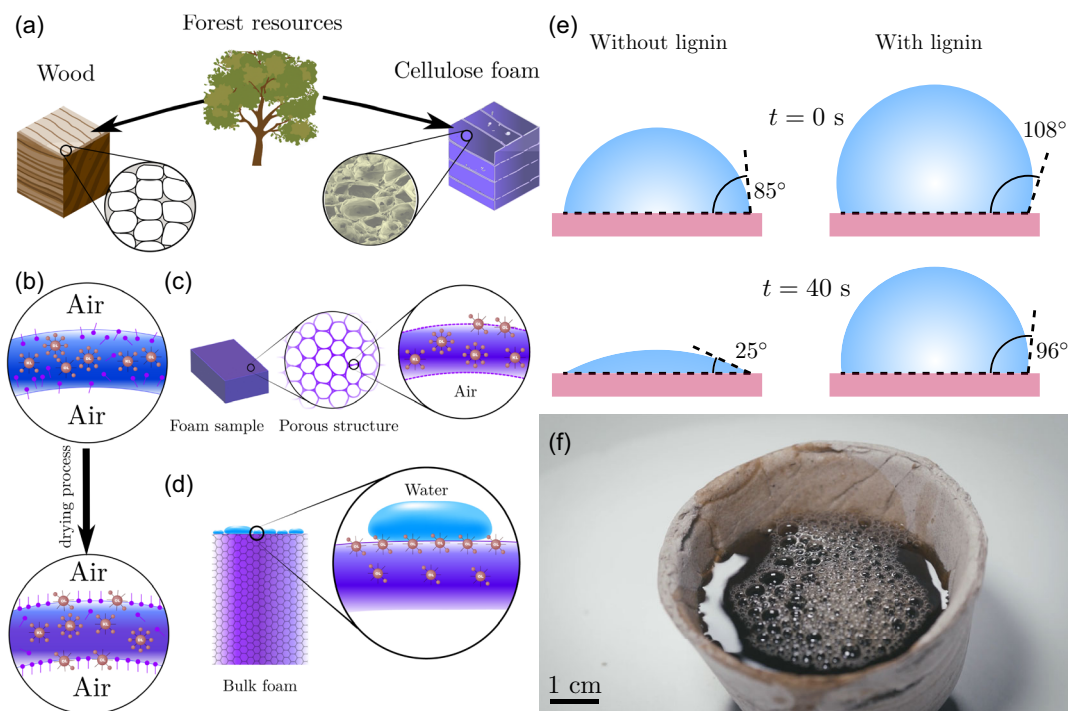


Figure 1. Biomimicry and lignin migration. a) The structure of wood was mimicked in the laboratory: in the lightweight cellular structure, the cellulose provides strength and lignin protection. b) During the drying process, water (blue) is removed, leaving a methylcellulose (MC) film (purple) doped with lignin particles (organosolv lignin [OL], dealkaline lignin [DL], and Kraft lignin [KL]). c) Depending on the surface chemistry, particles were located in different parts of the film. d) A water-resistant layer was created if the lignin particles migrated to the surfaces of the bubble films. e) An illustration of the contact angle behavior of a water droplet on the sample surface. In the hydrophilic material without lignin, the water was absorbed into the foam, decreasing the contact angle, but the same material with added lignin maintained the hydrophobic property overtime. f) A prototype edible coffee cup made out of the hydrophobic foam material.

properties of cellulose foams, as shown in Figure 1b–d. For example, ref. [29] reported a hydrophobic cellulose foam after driving hydrophobic silica particles to the air–liquid interfaces. However, ref. [16] used hydrophilic and hydrophobic surfactants to attract or repel cellulose fibers from the air–liquid interface. Since lignin comprises a combination of hydrophobic and hydrophilic end groups (e.g., methoxy, phenolic, and hydroxyl moieties), lignin particles can form Pickering systems.^[28,30–32] In other words, if the lignin particles inherit the properties of the lignin molecules, they ideally would reorient their hydrogen bonds toward the continuous liquid phase and their hydrophobic sides toward the air phase. In addition, by saturating the foam system with lignin particles, they would aggregate, giving rise to “lignin bumps” on the foam surface.^[11] Those bumps represent the surface roughness, thus reducing the solid–liquid contact area of the foam surface (Figure 2a).^[7,11,33–35] Both hydrophobic lignin groups and lignin bumps can favor the hydrophobic behavior of cellulose foams.

We began by taking a water-soluble cellulose derivative foam material^[11,12] and confirming what characteristics lignin should have to hydrophobize these methylcellulose (MC)-based foams. First, we evaluated the wettability of MC coatings containing different lignins: dealkaline lignin (DL),^[36] Kraft lignin (KL),^[37] and organosolv lignin (OL).^[38] With the best-performing lignin from the tests on the coatings, we examined the wetting behaviors of several foam biocomposites made from liquid-foam-templating

MC aqueous suspensions with various lignin contents. Our work exploits the amphiphilicity of lignin without further chemical modification, with the hypothesis that the colloidal behavior of lignin will drive its partially hydrophobic regions to the air–liquid interfaces and will remain stable since lignin and MC can partially cross-link.^[11,39] Depending on the number of hydrophobic groups, lignin will aggregate, modifying the surface chemistry and roughness of the foam surface, allowing it to function as it does in wood. Finally, we correlated the surface roughness—estimated from scanning electron microscopy (SEM) images with an image recognition and tracking algorithm—and the measured water absorption caused by capillary drainage to the measured water surface contact angles of MC/lignin foams (Figure 1e).

Our research showed that the addition of water-resistance properties to naturally hydrophilic and biodegradable materials presents an opportunity for their use in a variety of applications. In particular, our findings show that hydrophobizing cellulose foams with lignin creates an opportunity for the replacement of a wide range of plastic products, such as Styrofoam. To illustrate this, we present a prototype solution in the form of a single-use coffee cup made of hydrophobic foam (Figure 1f). This replacement not only successfully held coffee for several days, but it also disintegrated in cardboard recycling. Future material solutions may include carbon sinks for building insulation, foam meat trays, and protective packaging for electronics.

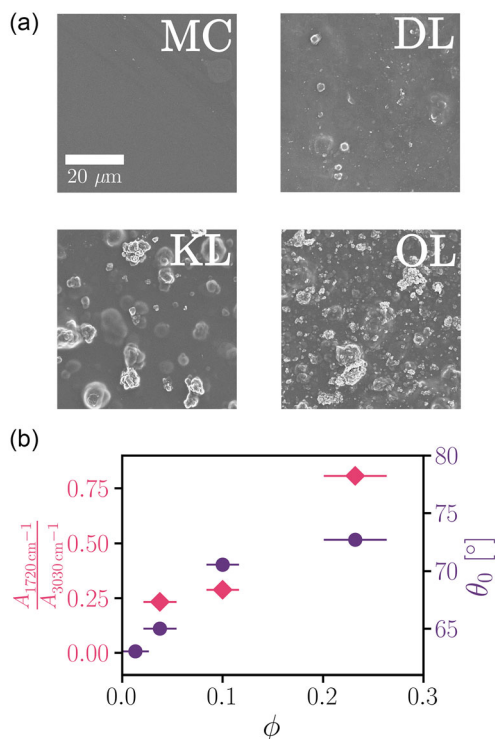


Figure 2. Spin-coating: a) scanning electron microscopy (SEM) images of spin-coated films illustrate that with DL, the lignin did not remain at the surface where KL and OL are clearly visible. b) Lignin Fourier-transform infrared (FTIR) spectroscopy absorbance values $A_{1720\text{ cm}^{-1}}$ (normalized by the value at 3030 cm^{-1}), as a measure of the number of hydrophobic groups present, correlated with the contact angle measurement θ_0 and the observed coverage of lignin at the surface ϕ for the materials seen in (a).

These findings contribute to advancing sustainable material alternatives that are both effective and environmentally conscious.

2. Results and Discussion

2.1. Spin-Coated Films

We produced hydrophobic cellulose foams with different types of lignins and varying lignin contents. Initially, we tested three lignins with the same concentration in MC suspensions, as well as a reference without lignin. These suspensions were deposited on silica wafers via spin-coating. We imaged the surface morphologies of the coatings formed on the silica wafers via SEM and correlated the coating roughness with its wettability (water contact angle). As the lignin concentration is kept constant, either the lignin stays in the bulk of the film and is not visible in the SEM images, or conversely a rough lignin-rich surface indicates the self-assembly of the lignin particles to the imaged surface instead of the bulk (see Figure 1c). We took the lignin with the best performance in terms of hydrophobicity (according to contact angle results) and made bulk foam blocks using different concentrations of said lignin. The same imaging and wettability studies performed on the spin-coated samples were also performed on the

bulk foams. From the exploratory results on silica wafers, OL showed the best performance, reaching the highest initial water contact angles. OL was thus chosen to fabricate biocomposite foam blocks based on the contact angle results on silica wafers.

The outstanding performance of OL over the DL and KL arose from the distribution of hydrophobic and hydrophilic groups in the lignin macrostructure. The best possible lignin would have had an optimal distribution of hydrophobic and hydrophilic groups, which would allow the hydrophobic groups to uniformly self-assemble to the sample surface. The ideal lignin has similar properties to that found in nature, which can be viewed as a physical hydrophobic barrier in the ultrastructure of wood. It is well known that isolating lignin via organosolv processing has a very mild influence on the original chemical structure of the native lignin, resulting in a structure with more hydrophobic groups.^[40–42] We have confirmed this with Fourier-transform infrared (FTIR) spectroscopy. Unlike nuclear magnetic resonance imaging, which is typically used to elucidate the lignin chemical structure, FTIR is a rapid and inexpensive technique for observing the differences between the OL, DL, and KL. The FTIR spectrum of the OL showed strong absorption at 1720 cm^{-1} (see Figure 4 and Table 1, Supporting Information). This absorption band corresponds to the C=O stretching vibrations in unconjugated ketones. Therefore, the OL retained more of the hydrophobic interaction characteristics of native lignin than the DL and KL. Further studies into the batch repeatability of these results should be carried out. The organosolv process preserves the ether linkages native to lignin, while the other processes tend to cleave these bonds, producing phenolic groups with an affinity to water.^[43] In a previous article,^[11] we discussed the appearance of an FTIR absorption band at 1720 cm^{-1} in a foam made of MC and lignin. This absorption band can potentially correspond to the carbonyl group formed due to esterification, suggesting that the manufacturing process of the foam, especially the drying at high temperatures, induces a chemical cross-linking between MC and lignin.^[39,44] This leads to the formation of ester-linkages in the polymeric network. We also pointed out the FTIR band at 1720 cm^{-1} in lignin, which corresponds to the C=O stretching band in unconjugated ketone. We acknowledge that future works should assess if the C=O reacts with the unsubstituted hydroxyl groups of MC, thus creating a chemically cross-linked composite. We remark that the cross-linking mechanism between lignin and MC requires more systematic studies that are beyond the scope of this article.

The sample surface microstructures can be seen in Figure 2a. The reference sample had a smooth-looking surface, while adding lignin made the surfaces rough. This was visible as quasi-spherical bumps on the sample surface observed in the SEM images, which were reminiscent of the surface features in the SEM image of pure lignin (Figure 3b, Supporting Information). We conjecture that the portion of each lignin considered partially hydrophobic was driven to form bumps or aggregates due to polymer–polymer interactions (hydrophobic interactions). At the same time, the hydrophilic parts were dispersed homogeneously in the MC coating formed on the silica wafer. The number of bumps varied with the different types of lignins used, and the OL was the substance with a higher tendency to form bumps. We also tracked the area fraction ϕ of the lignin bumps from the SEM images, and this quantity correlated with the

(normalized) height of the FTIR peak $A_{1720\text{ cm}^{-1}}/A_{3030\text{ cm}^{-1}}$, as shown in Figure 2b.

We performed sessile drop tests to measure the water contact angle on the foam-coated silica wafers. The true static contact angle on the absorbing surfaces was not defined, since the contact angle continuously shrank as the liquid became absorbed from the droplet into the material.^[45] This decrease in the contact angle occurred at roughly the same rate in all the samples (see Supporting Information). However, the initial contact angle correlated well with the area fraction of the lignin and therefore also with the FTIR peak at 1720 cm^{-1} , as shown in Figure 2b and 4, Supporting Information.

2.2. Foam Samples

Using the best-performing lignin from the spin-coating tests, bulk foam samples were produced. Similar to the spin-coated samples, the addition of lignin introduced surface roughness to the samples in the form of roughly spherical bumps, as seen in the SEM images (Figure 3a–k) of the sample surfaces. The number of bumps increased as the lignin concentration increased. Tracking the area fraction ϕ showed (Figure 3l) that it increased in a linear fashion with the lignin concentration in

the suspension C (black line in Figure 3l). This was consistent with the uniform dispersion of lignin (Experimental Section and Equation (4)) and means that with $C = 1\%$ we obtained $\phi = 27\%$. From the standard deviation of the area fraction ϕ shown in the error bars of Figure 3l, one can see that no large variations in the area fraction were seen between the SEM images, i.e., the lignin was distributed homogeneously on the surfaces.

We performed the same sessile drop tests for the bulk foam blocks. The droplets used in the tests were approximated as spherical caps with volumes

$$V = \frac{\pi r^3 (2 + \cos \theta)(1 - \cos \theta)^2}{3 \sin^3 \theta} \quad (1)$$

where r is the droplet baseline radius and θ is the contact angle. This can be exploited to determine the water absorption rate $K_a = -A^{-1} \partial V / \partial t$ as a function of the lignin concentration C . Here, we assumed capillary drainage, $K_a = \Delta P / (R_{\text{tot}} A)$, with area A , total flow resistance R_{tot} , and driving pressure ΔP .^[46] We included a constant evaporation rate K_∞ due to the experimental limitations. The flow of water went through the resistive layers of the lignin with the flow resistance R_L and bulk MC

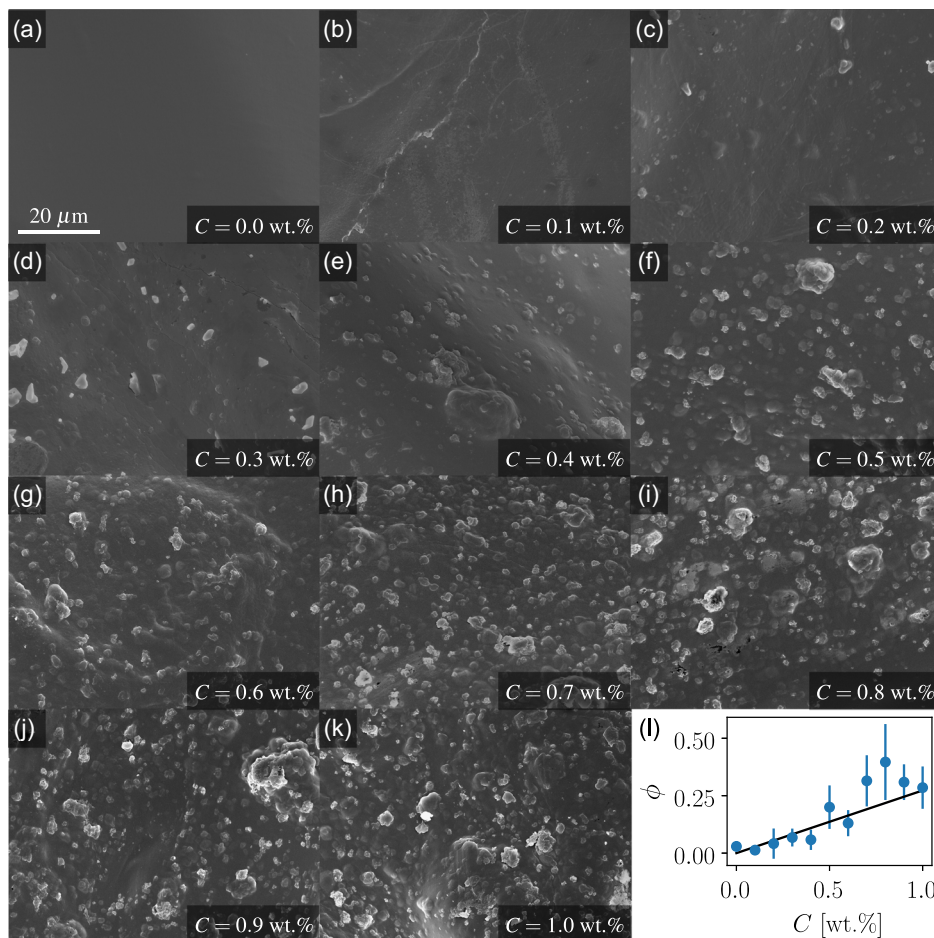


Figure 3. Effect of lignin concentration on the sample surfaces. a–k) SEM images of the samples with increasing lignin concentration C and equal MC concentration. l) The area fraction ϕ as a function of the lignin concentration C . The black line is the prediction from Equation (4).

(R_{MC}) in series. The water absorption rate K_a can be expressed (Experimental Section for the full derivation) as two flow resistors in series and, finally, with the help of the Kozeny–Carman equation,^[46–49] as

$$K_a = \frac{\Delta P}{A} (R_L + R_{MC})^{-1} + K_\infty \quad (2)$$

$$= \Delta K \left[\alpha \frac{\phi_0^2 C^2}{(1 - \phi_0 C)^3} + 1 \right]^{-1} + K_\infty$$

where $\Delta K = K_0 - K_\infty$, K_0 is the absorption rate of the pure MC foam, α is a fit parameter, and the linear relation $\phi = \phi_0 C$ was used. The fit parameter α included the hydrophobicity of the lignin as well as the geometry of the particles and their deposition, and it was directly related to the water resistance due to lignin particles relative to that of the pure MC, R_L/R_{MC} , in the foam structure.

Figure 4a shows the fit of Equation (2) to the experimental data. The resulting absorption rate of pure MC foam $K_0 = 11.4 \text{ mL} (\text{m}^2 \text{ s})^{-1}$ and the asymptotic evaporation rate $K_\infty = 1.75 \text{ mL} (\text{m}^2 \text{ s})^{-1}$ are shown as dashed lines. The only fit parameter had the value $\alpha = 487$. At $C = 1\%$, the ratio $R_L/R_{MC} = \alpha/\kappa = 91$ showed (Experimental Section for details) that the lignin layer provided a 91 times higher water resistance than that of the pure MC. Even a small amount of lignin, $C = 0.5 \text{ wt}\%$ in the suspension, dramatically increased the water resistance, as the absorption rate had already dropped by $(K_0 - K_a)/\Delta K = 95\%$, indicating that the material was hydrophobic.

The addition of lignin increased the initial contact angle θ_{i_0} , as can be seen in Figure 4b. The Cassie equation can be applied for a surface consisting of lignin (area fraction ϕ) and MC:

$$\cos \theta = \phi R_L \cos \theta_L + (1 - \phi) \cos \theta_0 \quad (3)$$

where R_L and θ_L are the roughness ratio and contact angle of a pure lignin surface, respectively, and θ_0 is the contact angle of the surface without lignin. This would indicate that the crossover from initially hydrophilic to initially hydrophobic surfaces ($\theta_{i_0} = 90^\circ$) occurred around $C = 0.5 \text{ wt}\%$. Note that this value also corresponded to the point highlighted in the previous paragraph, where the absorption rate was already close to the asymptotic value.

A more drastic effect was observed in the time evolution of the contact angle. The normalized contact angle θ/θ_{i_0} is shown in Figure 4c and clearly shows that foam blocks with suspension lignin concentrations $C < 0.2 \text{ wt}\%$ had very rapidly decreasing contact angles. However, with lignin concentrations above this level, the decrease in the contact angle during the experiment was only around 5%–20%.

By combining the Cassie equation (Equation (3)) for the initial state, the spherical cap approximation (Equation (1)), and the Kozeny–Carman capillary drainage model (Equation (2)) for water absorption, the time evolution of the contact angle was computed (Experimental Section for details). As an illustrative example, the contact angle θ at $t = 40 \text{ s}$ is shown in Figure 4d, as is the numerical result. The increase in the contact angle with increasing lignin concentration was clear, and the numerical approximation was very good. The change in the wetting physics from the lignin occurred already at relatively low coverage fractions when interpreted in this way. Our modeling effort implies that further hydrophobicity should be expected by adding more lignin.

In addition to the contact angle tests shown here, we performed simpler water column tests (see Supporting Information)

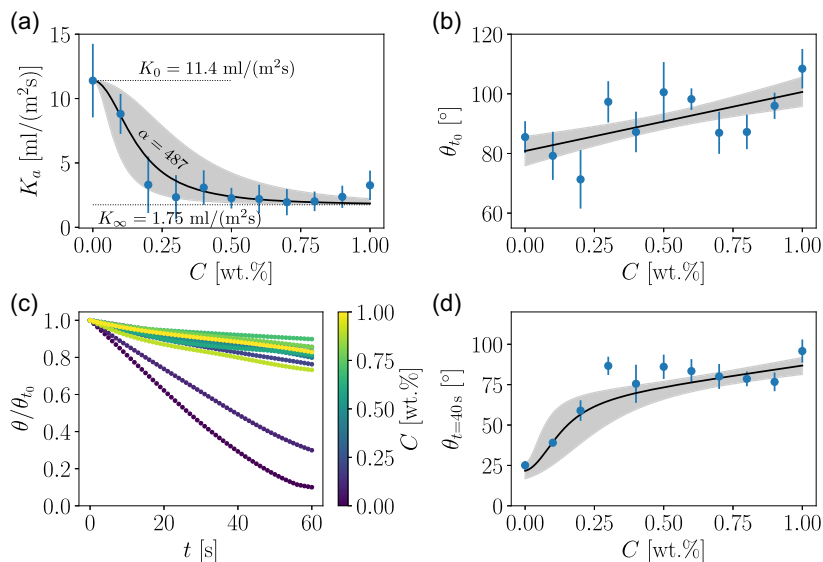


Figure 4. Effect of lignin concentration on the water absorption and the contact angle. a) The water absorption rate as a function of the lignin concentration in the suspension. The solid line represents a fit to Equation (2), and the shaded region shows the effect of changing the parameter α . The horizontal dashed lines correspond to the water absorption rates K_0 without lignin and the K_∞ asymptotic value. b) The initial contact angle θ_{i_0} as a function of the lignin concentration C . The black line corresponds to a fit to Equation (3). c) The normalized contact angle θ/θ_{i_0} as a function of time t , where the colors of the curves represent the lignin concentration C . d) The contact angle as a function of the lignin concentration at one point in time ($t = 40 \text{ s}$), as well as the result of numerically integrating Equation (5) (black line), which combines Equations (1)–(3).

to study the performances of lignin foams in wet environments. The water retention of a foam with 0.5 wt% lignin was 10 times better than that of a reference sample or cardboard. We also tested the mechanical properties (yield stress and Young's modulus) of the foam blocks in a humid environment and found that the lignin foams showed great improvements in retaining their properties (see Supporting Information).

We have also tested the feasibility of producing actual industrial-style end products, beyond the lab scale, using the hydrophobization method described earlier. A replacement for a single-use Styrofoam cup was made (see Figure 1f and Supporting Information), and it performed as well as other industry alternatives for drinking coffee.

3. Conclusion

We have presented a successful attempt at biomimicry, where the structure and chemical composition of wood were used as an inspiration for MC foams, to yield water-resistance properties tunable by lignin addition. Achieving such water resistance required evaluating how the complex chemical structure of lignin affected its migration in the liquid films of the bio-based foams. Our results showed that fully bio-based and biodegradable foams with sufficient water resistance for practical applications are attainable with scalable processes. Therefore, our bio-based material is a prime candidate for a plastics substitute—a field where up-scalable, economically viable, and ready-for-practical-use solutions are desperately needed.

Furthermore, our findings demonstrate the synergy between OL and cellulose-based substrates to produce hydrophobic bio-based materials via chemical cross-linking. We assessed three different types of lignin and, from FTIR measurements, deduced that OL has the greatest potential for increasing hydrophobicity. The lignin properties result from the distribution of hydrophobic and hydrophilic groups in the lignin macromolecular structure; the OL retained more of the hydrophobic interactions present in native lignin than the other types of lignin tested (DL and KL). We tested this, making spin-coated samples using the foam suspension, viewing the lignin surface aggregation via SEM and correlating the FTIR measurements and the SEM area fractions with the initial contact angle in water droplet tests. The spin-coated samples were used as a comparison to elucidate the interfacial phenomena and wetting interactions in bulk foam samples.

Adding lignin to the bulk foam samples produced surface morphologies indicating that, although the lignin self-assembles to the bubble film surfaces, it is uniformly distributed in whole bulk foam block. The addition of lignin also increased the initial contact angles of the bulk foam blocks to the hydrophobic range. The decrease in the contact angle with time was also significantly reduced. The time evolution of the contact angle could be explained with just three components: the wettability of the initial rough surface with lignin and MC obtained using the Cassie equation (Equation (3)), the spherical cap approximation (Equation (1)), and the water absorption by capillary drainage obtained using the Kozeny–Carman equation (Equation (2)).

We additionally performed simple water column tests and observed that the addition of lignin improved the water retention by a factor of 10 and the lignin foam outperformed standard

packaging solutions, such as cardboard. The mechanical properties in humid environments were also retained longer when lignin was added to the foam.

To demonstrate how to move out of the lab scale, we have also made prototypes of the foam end products and found that these performed as well as industry alternatives, as the cup in Figure 1f illustrates. To summarize, our biomimicry approach resulted in foams with hydrophobic properties for practical plastic-substitution purposes. The desired properties were achieved by including lignin directly in the templating of the foam blocks without any post-processing methods.

4. Experimental Section

For all the experiments, we employed food-grade MC purchased from Ashland Specialties, Belgium. The MC had a degree of substitution for CH_3 of 1.87, polydispersity index of 1.50, and weight average molecular weight of 534 kg mol^{-1} .^[50] We used three lignins: KL, OL, and DL. Softwood KL called BioPiva 100 (molecular weight $M_w = 5000 \text{ g mol}^{-1}$) was provided by UPM Biochemicals (Finland). Wheat-straw-derived OL ($M_w = 3108 \text{ g mol}^{-1}$) came from a pilot plant that extracts lignin from agricultural crops. DL was a commercial hardwood lignin purchased from Biosynth Carbosynth (UK). The densities of the different lignins and MC samples were determined by a gas pycnometer (Ultrapyc 1200e, Quantachrome, USA). A 10 cm^3 measurement cell was filled with the material prior to being pressurized with helium gas. All measurements were repeated 15 times, and the densities were subsequently calculated based on Boyle's law using an average of the 10 most correlated data points. From this procedure, the density of MC was measured as $\rho_{\text{MC}} = 1322.7 \text{ kg m}^{-3}$, while for the lignins, the densities were $\rho_{\text{KL}} = 1286.9 \text{ kg m}^{-3}$ (KL), $\rho_{\text{OL}} = 1346.8 \text{ kg m}^{-3}$ (OL), and $\rho_{\text{DL}} = 1486.2 \text{ kg m}^{-3}$ (DL). The standard deviation of the density measurements was $\Delta\rho \leq 2.0 \text{ kg m}^{-3}$ in all cases. The solvent was high-quality tap water with the properties reported in ref. [50].

FTIR Spectroscopy: Infrared spectra of the technical lignins were obtained using a Spectrum Two LiTaO₃ spectrometer (Perkin Elmer, UK) equipped with an attenuated total reflection (Specac Quest, UK) accessory. The spectra were acquired within a wavelength range of $4000\text{--}500 \text{ cm}^{-1}$ at room temperature. The acquisition resolution was 4 cm^{-1} , and 30 scans were performed. The results presented here required no baseline correction. The experiments were replicated to confirm the shapes of the spectra. See Supporting Information for additional details on the FTIR spectra peaks.

Spin-Coating: Before preparing bulk foam samples, we spin-coated silicon wafers separately with suspensions containing 0.25 wt% of each type of lignin and 0.9 wt% of MC. A reference sample without lignin was included in the analysis. The silicon wafers were coated using a WS-650SX-6NPP/LITE spin-coater (Laurell Technologies). Each coated sample contained 10 layers of a thin film so that the coating would be thick enough for the contact angle measurements. Each layer was produced similarly using 4000 rpm and 10 s as the spinning time. The solution was added to the silicon substrate with a pipette. After one layer was coated, the film was allowed to dry fully at room temperature, after which another layer was coated.

Foam Preparation: According to Table 1, MC powder was dispersed in 80 g of tap water at 60 °C. After the MC was fully dispersed in water, lignin was added to the solution. Finally, more tap water was added to ensure the suspension's total weight reached 100 g. The suspensions were tempered at 3 °C for 24 h. We prepared 11 suspensions with different OL concentrations in the suspension, ranging from 0 to 1.0 wt%. We foamed the suspension using the Tessari method. We connected two syringes using a plastic tube. One syringe contained 15 mL of the suspension, and the other was adjusted to a free volume of 15 mL. A wet foam was produced by exchanging the suspension from one syringe to another several times until the foam volume was doubled. After this, the wet foam was extruded using

Table 1. Concentrations by weight of MC C_{MC} , OL C , and water C_W in the suspensions used for the tested foam samples.

Sample	C_{MC} [wt%]	C [wt%]	C_W [wt%]
Foam-1	1.8	0.1	98.1
Foam-2	1.8	0.2	98.0
Foam-3	1.8	0.3	97.9
Foam-4	1.8	0.4	97.8
Foam-5	1.8	0.5	97.7
Foam-6	1.8	0.6	97.6
Foam-7	1.8	0.7	97.5
Foam-8	1.8	0.8	97.4
Foam-9	1.8	0.9	97.3
Foam-10	1.8	1.0	97.2

a syringe and was continuously dried for 2 h with a heating lamp. The process has been described in more detail in ref. [11].

SEM: We observed the surfaces of the foams and silicon wafers via SEM. For the analysis, we sputter-coated the samples with a thin layer of Au/Pd 80/20 and mounted them on carbon conductive tape. We used a field-emission SEM from Zeiss Sigma VP (Germany) and applied an electric potential of 5 keV. The images were taken using the type II secondary electrons (SE2) signal. At least 40 images were taken for each lignin concentration (10 for the reference sample without lignin).

The bumps seen in the SEM images were tracked using a method (see, e.g., Figure 3a) based on thresholding the image intensity gradient magnitude: $\sqrt{\left(\frac{\partial I}{\partial x}\right)^2 + \left(\frac{\partial I}{\partial y}\right)^2}$, where I is the image intensity and x and y are the spatial coordinates in the image. The (filled) connected components in the binary image produced by thresholding were extracted. If their roundness, defined as $\sqrt{4\pi A/p}$, where A is the area of the connected component and p is the perimeter, exceeded a value of 9%, the component was considered a bump. This filtering by roundness was done to exclude some clearly non-bump features (e.g., ridges) from the analysis. The area fraction ϕ of the bumps was then simply the area of the bumps in the image divided by the size of the image.

In the case of foam blocks, if the lignin was uniformly distributed in the sample, the area fraction ϕ of the lignin on the foam surface equaled the volume fraction of lignin in the block V_L/V_B , where V_L is the volume occupied by the lignin and V_B is the volume of the block. The dependence of the volume fraction on the lignin concentration C by weight in the suspension was determined to be

$$\phi = \frac{V_L}{V_B} = \frac{\rho_B^{\text{ref}} C}{\rho_L C_{MC}} = \phi_0 C \quad (4)$$

where ρ_B^{ref} is the density of the reference block without lignin, ρ_L is the density of the lignin, and C_{MC} is the MC concentration by weight in the suspension. Based on the measured densities, we obtained $\phi_0 = 27.28$.

Sessile Water Droplet: The wettability of the foam surfaces and silicon wafers was measured using the water contact angle θ on a Theta Flex tensiometer (Biolin Scientific, Sweden). For the test, a drop of $5.5 \pm 0.9 \mu\text{L}$ of water (resistivity of $18 \text{ M}\Omega \text{ cm}$) was deposited on the top surface of the selected substrate. The contact angle of each sample was measured once every second for 1–5 min. Each measurement was taken in at least triplicate. Figure 1 and Figure 1, Supporting Information, show a visual examples of the contact angle test.

Numerical Computation of Contact Angle Time Evolution: As the droplets used were small (around $5 \mu\text{L}$), the gravity effects could be neglected, and the droplet could be approximated as a spherical cap with a volume given

by Equation (1). This approximation enabled the computation of the absorption rate $K_a = (-1/A)(dV/dt)$, where $A = \pi r^2$ is the area of the droplet base. If the absorption rate K_a was known and assumed to be only a function of the lignin concentration C in the suspension, the contact angle at time t could be integrated from a relation derived by differentiation of Equation (1):

$$\frac{d\theta}{dt} = \frac{\sin \theta}{r} \left[\frac{\sin^3 \theta}{(1 - \cos \theta)^2} K_a(C) - (2 + \cos \theta) \frac{dr}{dt} \right] \quad (5)$$

where the absorption rate is explicitly present. Here, we also included the increase in the droplet radius (see Supporting Information for more details), although the effect was small.

Flow Rate through Particle-Laden Matrix: Capillary Drainage: We assumed that the flow of water through the material could be described with a hydrodynamic resistance to the driving pressure: $\Delta P = R_{\text{tot}} Q$, where R_{tot} is the total resistance of our binary material and $Q = -dV/dt$ is the flow rate. Thus, the absorption rate K_a , the rate of water volume loss per droplet base area or contact area A , could be expressed as the sum of the flow rate through the foam and the constant evaporation rate per area K_∞ .

$$K_a = -\frac{1}{A} \frac{dV}{dt} = \frac{Q}{A} + K_\infty = \frac{\Delta P}{R_{\text{tot}} A} + K_\infty \quad (6)$$

We assumed that no significant amounts of water entered the high MC concentration foam, and thus, we approximated the value of K_∞ directly from our K_a versus the lignin concentration data.

The total resistance R_{tot} had two parts in series: R_L from the dense particle-covered surface and R_{MC} from the bulk MC matrix below. The resistance caused by the particles could be expressed by the Kozeny–Carman equation,^[46–49] which described the permeability of a porous medium κ or the flow resistance due to a dense particle layer $R_L \propto 1/\kappa$ as a function of the porosity $\varepsilon = 1 - \phi$, where ϕ is the area fraction of the lignin particles obtained from the SEM images. For simplicity and to reduce experimental noise, we used the measured relation between particles on the surface and the concentration of particles in the suspension: $\phi = \phi_0 C$ (computed in Equation (4) and shown in Figure 3), leading to the permeability

$$\kappa = \frac{\varepsilon^3}{(1 - \varepsilon)^2} = \frac{(1 - \phi_0 C)^3}{\phi_0^2 C^2} \quad (7)$$

and flow resistance $R_L = R_0 \phi_0^2 C^2 / (1 - \phi_0 C)^3$, where the prefactor R_0 includes the geometric aspects of the particles.^[49]

Finally, we obtained an equation for the measurable quantity K_a , the rate of water volume loss of the droplet on the surface per droplet base area A , as

$$K_a = \frac{\Delta P}{A} (R_L + R_{MC})^{-1} + K_\infty = \frac{\Delta P}{R_{MC} A} \left[\frac{R_0}{R_{MC}} \frac{\phi_0^2 C^2}{(1 - \phi_0 C)^3} + 1 \right]^{-1} + K_\infty \quad (8)$$

which directly leads to Equation (2) by setting $\Delta K = K_0 - K_\infty = \Delta P / (R_{MC} A)$ and $\alpha = R_0 / R_{MC}$. The fit parameter α directly relates to the relative resistance of the lignin particles compared with that of the pure MC through $R_L / R_{MC} = \alpha / \kappa$. In our case, this means that the relative lignin resistances we observed were between zero (for $C = 0\%$) and 0.19α (for $C = 1\%$, i.e., $\phi = 0.27$).

Supporting Information

Supporting Information is available from the Wiley Online Library or from the author.

Acknowledgements

The authors thank Benjamin Wilson for determining the powder densities. M.J.A. and J.K. acknowledge the support from FinnCERES flagship (grant no. 151830423), Business Finland (grant no. 211835), and Future Makers. M.J.A., T.M., and I.Y.M.-V. acknowledge the support from Business Finland (grant no. 211909). J.K. acknowledges funding from the Academy of Finland (grant no. 308235). M.J.A. acknowledges support from the Academy of Finland (Center of Excellence program (program nos. 278367 and 317464). The authors acknowledge Woamy Oy (Finland) for providing the MC. The authors acknowledge the computational resources provided by the Aalto University School of Science "Science-IT" project and the provision of facilities and technical support by Aalto University at OtaNano–Nanoscience Center (Aalto-NMC).

Conflict of Interest

A patent application for the hydrophobization of wood-like foam has been submitted. No other conflicts of interest exist.

Data Availability Statement

The data that support the findings of this study are available from the corresponding author upon reasonable request.

Keywords

biomimicries, celluloses, hydrophobics, lignins

Received: January 29, 2024

Revised: July 17, 2024

Published online: August 3, 2024

- [1] European Commission, *Off. J. Eur. Union* **2019**, 62.
- [2] D. Klemm, B. Heublein, H.-P. Fink, A. Bohn, *Angew. Chem. Int. Ed.* **2005**, 44, 3358.
- [3] T. Li, C. Chen, A. H. Brozyna, J. Y. Zhu, L. Xu, C. Driemeier, J. Dai, O. J. Rojas, A. Isogai, L. Wågberg, L. Hu, *Nature* **2021**, 590, 47.
- [4] T. Hjelt, J. A. Ketoja, H. Kiiskinen, A. I. Koponen, E. Pääkkönen, *J. Dispersion Sci. Technol.* **2021**, 43, 1462.
- [5] B. Wicklein, A. Kocjan, G. Salazar-Alvarez, F. Carosio, G. Camino, M. Antonietti, L. Bergström, *Nat. Nanotechnol.* **2015**, 10, 277.
- [6] R. Li, J. Du, Y. Zheng, Y. Wen, X. Zhang, W. Yang, A. Lue, L. Zhang, *Cellulose* **2017**, 24, 1417.
- [7] E. S. Ferreira, E. D. Cranston, C. A. Rezende, *ACS Sustainable Chem. Eng.* **2020**, 8, 8267.
- [8] A. Ottenhall, T. Seppänen, M. Ek, *Cellulose* **2018**, 25, 2599.
- [9] C. Debeleac, P. Nechita, S. Nastac, *Polymers* **2019**, 11, 1223.
- [10] C. Chen, Y. Zhou, W. Xie, T. Meng, X. Zhao, Z. Pang, Q. Chen, D. Liu, R. Wang, V. Yang, H. Zhang, H. Xie, U. H. Leiste, W. L. Fourney, S. He, Z. Cai, Z. Ma, T. Li, L. Hu, *Adv. Funct. Mater.* **2023**, 33, 2204219.
- [11] I. Y. Miranda-Valdez, S. Coffeng, Y. Zhou, L. Viitanen, X. Hu, L. Jannuzzi, A. Puisto, M. A. Kostianen, T. Mäkinen, J. Koivisto, M. J. Alava, *Cellulose* **2023**, 30, 2253.
- [12] M. Reichler, S. Rabensteiner, L. Törnblom, S. Coffeng, L. Viitanen, L. Jannuzzi, T. Mäkinen, J. R. Mac Intyre, J. Koivisto, A. Puisto, M. J. Alava, *Sci. Rep.* **2021**, 11, 24306.
- [13] K. Ganesan, A. Dennstedt, A. Barowski, L. Ratke, *Mater. Des.* **2016**, 92, 345.
- [14] P. Giachini, S. Gupta, W. Wang, D. Wood, M. Yunusa, E. Baharlou, M. Sitti, A. Menges, *Sci. Adv.* **2020**, 6, eaay0929.
- [15] T. Mäkinen, J. Koivisto, E. Pääkkönen, J. A. Ketoja, M. J. Alava, *Soft Matter* **2020**, 16, 6819.
- [16] A. E. Ketola, W. Song, T. Lappalainen, K. Salminen, J. Viitala, T. Turpeinen, A. Miettinen, K.-Y. Lee, J. A. Ketoja, *ACS Appl. Polym. Mater.* **2022**, 4, 7685.
- [17] G. Glenn, W. Orts, A. Klamczynski, R. Shogren, W. Hart-Cooper, D. Wood, C. Lee, B.-S. Chiou, *Cellulose* **2023**, 30, 3489.
- [18] L. Viitanen, I. Y. Miranda-Valdez, J. Koivisto, A. Puisto, M. Alava, *Cellulose* **2023**, 30, 4215.
- [19] J. R. Mac Intyre, D. Raka, M. Aydin, L. Viitanen, J. Koivisto, *J. Mater. Sci.* **2022**, 57, 11663.
- [20] Q. Liu, L. Luo, L. Zheng, *Int. J. Mol. Sci.* **2018**, 19, 335.
- [21] N. Kaushal, A. K. Singh, *Int. J. Biol. Macromol.* **2023**, 246, 125709.
- [22] S. Chen, Q. Shao, L. Hu, Z. Tan, D. Zheng, *J. Water Process Eng.* **2023**, 52, 103503.
- [23] X. Wang, X. Yang, Z. Wu, X. Liu, Q. Li, W. Zhu, Y. Jiang, L. Hu, *Polymers* **2023**, 15, 1316.
- [24] S. Yu, M. Wang, Y. Xie, W. Qian, Y. Bai, Q. Feng, *Int. J. Biol. Macromol.* **2023**, 233, 123598.
- [25] B. Cui, L. Liu, S. Li, W. Wang, L. Tan, C. Liu, W. Wang, *Mater. Chem. Front.* **2023**, 7, 897.
- [26] K. Mobredi, I. Y. Miranda-Valdez, T. Mäkinen, J. Koivisto, M. J. Alava, *Soft Matter* **2024**, 20, 5607.
- [27] M. Y. Balakshin, E. A. Capanema, I. Sulaeva, P. Schlee, Z. Huang, M. Feng, M. Borghei, O. J. Rojas, A. Potthast, T. Rosenau, *ChemSusChem* **2021**, 14, 1016.
- [28] C. Hansen, A. Björkman, *Holzforschung* **1998**, 52, 335.
- [29] R. Abidnejad, M. Beaumont, B. L. Tardy, B. D. Mattos, O. J. Rojas, *ACS Nano* **2021**, 15, 19712.
- [30] *Biopolymeric Nanomaterials: Fundamentals and Applications* (Eds: L. Klapiszewski, In S. Kanwar, A. Kumar, T. A. Nguyen, S. Sharma, Y. Slimani), Elsevier, Amsterdam **2021**, pp. 99–132.
- [31] S. Lam, K. P. Velikov, O. D. Velez, *Curr. Opin. Colloid Interface Sci.* **2014**, 19, 490.
- [32] Y. Yang, Z. Wei, C. Wang, Z. Tong, *Chem. Commun.* **2013**, 49, 7144.
- [33] Y. Y. Nam, W. Chao, in *MATEC Web of Conf.*, EDP Sciences, Nanjing, China vol. 275, **2019**, p. 01008.
- [34] C. Yang, U. Tartaglino, B. Persson, *Phys. Rev. Lett.* **2006**, 97, 116103.
- [35] J. Wang, H. Chen, T. Sui, A. Li, D. Chen, *Plant Sci.* **2009**, 176, 687.
- [36] R. Shu, J. Long, Y. Xu, L. Ma, Q. Zhang, T. Wang, C. Wang, Z. Yuan, Q. Wu, *Bioresour. Technol.* **2016**, 200, 14.
- [37] K. A. Henn, N. Forsman, T. Zou, M. Österberg, *ACS Appl. Mater. Interfaces* **2021**, 13, 34793.
- [38] P. J. De Wild, W. J. Huijgen, R. J. Gosselink, *Biofuels, Bioprod. Biorefin.* **2014**, 8, 645.
- [39] F.-Z. El Bouchtaoui, E.-H. Ablouh, M. Mhada, I. Kassem, M. H. Salim, S. Mouhib, Z. Kassab, H. Sehaqui, M. El Achaby, *Int. J. Biol. Macromol.* **2022**, 221, 398.
- [40] A. Lisý, A. Ház, R. Nadányi, M. Jablonský, I. Šurina, *Energies* **2022**, 15, 6213.
- [41] M. Kienberger, S. Maitz, T. Pichler, P. Demmelmayr, *Processes* **2021**, 9, 804.
- [42] *Bioenergy Research: Advances and Applications* (Eds: A. Berlin, M. Balakshin, V. K. Gupta, M. G. Tuohy, C. P. Kubicek, J. Saddler, F. Xu), Elsevier, Amsterdam **2014**, pp. 315–336.
- [43] I. Haq, P. Mazumder, A. S. Kalamdhad, *Bioresour. Technol.* **2020**, 312, 123636.
- [44] M. Hasanin, A. M. Labeeb, *Mater. Sci. Eng.: B* **2021**, 263, 114797.
- [45] S. Krainer, U. Hirn, *Colloids Surf., A* **2021**, 619, 126503.

- [46] S. Das, H. Patel, E. Milacic, N. Deen, J. Kuipers, *Phys. Fluids* **2018**, *30*, 012112.
- [47] J. Kozeny, *Sitzungsberichte der Akademie der Wissenschaften – Mathematisch-naturwissenschaftliche Klasse* **1927**, 126, 271.
- [48] P. C. Carman, *Trans. Inst. Chem. Eng.* **1937**, *15*, 150.
- [49] J. Koivisto, D. J. Durian, *Nat. Commun.* **2017**, *8*, 15551.
- [50] I. Y. Miranda-Valdez, L. Viitanen, J. M. Intyre, A. Puisto, J. Koivisto, M. Alava, *Carbohydr. Polym.* **2022**, *298*, 119921.